The approach described above can also be applied to refine the analysis for the internal stresses in three-dimensional composites. However, the difference in results calculated by the equations corresponding to the first and second approximations [Eq. (A20) vs Eq. (A31)] is small as shown in Fig. 10. The stress distribution along lines *ab* and *bc* (see Fig. 1) is shown in Fig. 15.

References

[1] Fil'shtinskii, L. A., "Stresses and Displacements in an Elastic Sheet Weakened by a Doubly-Periodic Set of Equal Circular Holes," *Prikladnaia Mathematika i Mekhanika*, Vol. 28, No. 3, 1964, pp. 430–441.

[2] Adams, D. A. and Doner, D. R., "Transverse Normal Loading on a Unidirectional Composite," *Journal of Composite Materials*, Vol. 1, No. 2, 1967, pp. 152–164.

[3] Adams, D. A. and Doner, D. R., "Longitudinal Shear Loading of a Unidirectional Composite," *Journal of Composite Materials*, Vol. 1, No. 1, 1967, pp. 4–18.

[4] Pickett, G., "Elastic Moduli of Fiber Reinforced Plastic Composites," *Fundamental Aspects of Fiber Reinforce Composites*, edited by R. T. Schwartz, Interscience, New York, 1968, pp. 13–27.

[5] Shaffer, B. W., "Elasto-Plastic Stress Distribution Within Reinforced Plastics Loaded Normal to Its Internal Filaments," *AIAA Journal*, Vol. 6, No. 12, 1968, pp. 2316–2324.

[6] Foye, R. B., "Structural Composites, Quarterly Progress Repts. 1 and 2, "USAF Contract AF 33(615)-5150, 1966, Air Force Materials Lab., Wright-Patterson Air Force Base, Ohio.

[7] Wilson, H. B., "Mathematical Studies of Composite Materials," S-42, Dec. 1963, Rohm and Haas Co., Huntsville Ala.

[8] Goodier, J. N., "A Survey of Some Recent Researches in Theory of Elasticity," *Applied Mechanics Review*, Vol. 4, 1951, pp. 330–332.

[9] Eshelby, J. D., "Elastic Inclusions and Inhomogeneities," *Progress in Solid Mechanics*, Vol. 2, North Holland Publishing, Amsterdam, 1961, pp. 89–140.

[10] Sternberg, E., "Three-Dimensional Stress Concentrations in the Theory of Elasticity," *Applied Mechanics Review*, Vol. 1, 1958, pp. 1–4.

[11] Sternberg, E., "On Some Recent Developments in the Linear Theory of Elasticity," *Structural Mechanics*, Pergamon Press, New York, 1960, pp. 48–73.

[12] Daniel, I. M. and Durelli, A. J., "Photoelastic Investigation of Residual Stresses in Glass Plastic Composites," *Proceedings of the 16th Annual Conference of the Society of Plastics Industry*, Sec. 19A, 1961.

[13] "Structural Airframe Applications of Advanced Composites; Fourth Quarterly Progress Report," AFML Contract AF33(615)-5257, June 1967, ITT Research Inst., Texaco Experiment, Inc., and General Dynamics.

[14] "Study of Mechanical Properties of Solid Rocket Grains," Rept. 0411-10F, prepared under contract AF33(600)-40314S. A. No. 1, March 1962, Aerojet General.

[15] Greszczuk, L. B., "Thermoelastic Properties of Filamentary Composites," *6th AIAA Structures and Materials Conference*, Palm Springs, Calif., 1965.

[16] Paul, B., "Prediction of Elastic Constants of Multiphase Materials," *Transactions* AIME, Vol. 218, 1960, p. 36.

[17] Ekvall, J. C., "Elastic Properties of Orthotropic Monofilament Laminates," Paper 61-AV-56, *Proceedings of ASME Aviation Conference*, Los Angeles, Calif., 1961,

[18] Greszczuk, L. B., "Elastic Constants and Analysis Methods for Filament Wound Shell Structures," Rept. SM-45849, Jan. 1964, Douglas Aircraft Co.

JULY 1971 AIAA JOURNAL VOL. 9, NO. 7

A Study of Hypersonic Corner Flow Interactions

RALPH D. WATSON* AND LEONARD M. WEINSTEIN†
NASA Langley Research Center, Hampton, Va.

Characteristics of the hypersonic flowfields over three sharp leading-edge internal corner models have been measured at Mach 20 in helium. Wedges of equal angles (0°–0°, 5°–5°, and 10°–10°) intersecting at 90° formed the models. The measurements include heat-transfer and surface pressure distributions, Pitot surveys in the base plane of the models, oil-flow photographs, and electron beam flow visualization photographs. The data indicate that the broad features of external and internal shock structure observed at supersonic Mach numbers also occur at Mach 20; however, the presence of large vortices and thick boundary layers distort the flow in the immediate vicinity of the corner. Observed peaks in surface heat transfer correlate with a strong vortex near the corner and a disturbance propagated from the inviscid flow into the boundary layer. The flowfield appears to be basically conical in nature except for large values of $\bar{\chi}$ the hypersonic viscous interaction parameter. Corner heating rates, relative to undisturbed wedge or flat-plate heating rates, increase significantly with increasing freestream Mach number.

Nomenclature‡

C = Chapman-Rubesin constant
M = Mach number
P = pressure
Pr = Prandtl number
$\dot{q}$ = heat flux
R = Reynolds number
T = temperature
x,y,z = Cartesian coordinates
$\bar{y},\bar{z}$ = orthogonal coordinates measured from the corner juncture
α = angle between wedge and freestream vector
γ = ratio of specific heats
δ = Pitot boundary-layer thickness
δ^* = displacement thickness
ϕ = wedge intersection angle, measured in y-z plane
$\bar{\chi}$ = viscous interaction parameter

Presented as Paper 70-227 at the AIAA 8th Aerospace Sciences Meeting, New York, January 19–21, 1970; submitted March 2, 1970; revision received March 15, 1971.

* Aerospace Engineer, Hypersonic Vehicles Division. Member AIAA.
† Aerospace Engineer, Hypersonic Vehicles Division.

‡ Primes denote reference temperature value.

Subscripts

c = calculated value
L = based on maximum x length
m = measured value
max = peak value
p = Pitot value
T = stagnation value
W = wedge value, including viscous interaction effects
x = based on distance x
FP = flat-plate value, including viscous interaction effects
∞ = freestream value

Introduction

THE corner flow problem, because of its practical importance, has given rise to a large number of experimental and theoretical studies in recent years.[1–16] Several classes of configurations have been investigated, from simple sharp leading-edge flat plates intersecting at right angles to more complex bodies having leading-edge bluntness effects, sweep, unsymmetrical wedge angles, and various intersection angles. Mach numbers have ranged from 2.5 to 16, and boundary layers have been both laminar and turbulent.

In spite of the amount of information which has accumulated, the flowfield is not well understood. It has been divided into near-corner and far-corner regions in Ref. 6, the near corner being the region immediately adjacent to the corner juncture, extending laterally to where a sharp drop in surface pressure occurs. The far-corner region is characterized by complicated shock interactions and internal flowfield disturbances at high Reynolds numbers, as well as by viscous interactions at low Reynolds numbers.

In early analyses of the inviscid flow, the wedge shocks were assumed to be planar up to their line of intersection,[5,17] but more recent work has shown that this is not generally true. The flowfield survey of Ref. 10 showed the presence of an intermediate corner shock joining two wedge shocks at Mach 3.17 for wedge angles of 12.2°. Korkegi's later calculations indicated the wedge shocks could not intersect in most cases[14] and proposed that the most general case consists of a corner shock joining the two wedge shocks. Based on the internal shock model of Ref. 10, a theoretical iteration scheme was devised to determine the location of an internal shock and thus the inviscid characteristics of the flowfield.[16]

A solution for the corner boundary layer in laminar compressible flow was developed using an integral approach.[3] This solution is accurate for corner intersection angles between 60° and 120°. A later analysis for incompressible flow more correctly considered the boundary conditions of the problem.[8] An extension of this work to compressible flows[9] showed that compressibility increases the secondary crossflow. The latest development is a theoretical solution to the problem by Rudman and Rubin[13] which calculates the entire flowfield between the shock and the body, including viscous effects. Experimental evidence of secondary flows for incompressible turbulent boundary layers can be found in Refs. 18 and 19.

Most corner configurations occurring on flight vehicles contain unsymmetrical intersections, leading-edge bluntness, boundary-layer buildup before the surface juncture occurs, and leading-edge sweep. However, in the simplest geometrical case of all, that of sharp wedges intersecting symmetrically, the flowfield details are not well known. In an attempt to clarify further simple corner flows at hypersonic Mach numbers, where appreciable viscous-inviscid interactions occur, an experimental program was conducted at Mach 20 in the Langley 22-in. helium tunnel. Model wedge angles were 0°, 5°, and 10° intersecting at 90°, and freestream Reynolds numbers based on maximum model length varied from about 1.3×10^6 to 6.7×10^6, giving predominantly laminar flow over the models. Heat-transfer and surface pressure distributions, flowfield Pitot surveys, and oil-flow and electron beam flow visualization photographs were obtained. (Some results for the 10° wedge corner were presented in Ref. 20.) Data from other sources are compared with the present results.

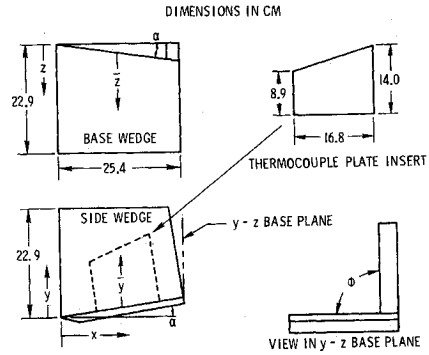

Fig. 1 Sketch of model with coordinate system.

Model and Coordinate System

The model consisted of two sharp leading-edge wedges intersecting at a 90° angle, symmetrical about a midplane through the intersection juncture. The steel base plate was pivoted so that it could be set at 0°, 5°, and 10° incidence to the flow: this plate contained pressure orifices. Side plates (separate sections constructed for each angle of attack) consisted of a metal frame coated with a 1.3-cm-thick layer of Fiberglas-impregnated resin. After making oil-flow studies, cavities were machined in each plate to receive a heat-transfer insert containing thermocouples. The heat-transfer inserts were installed flush with the side plate surface. End plates attached to the base and side plates minimized outflow effects. A sketch of the model including basic dimensions and the coordinate system used is shown in Fig. 1.

A 10-tube Pitot rake designed for detailed surveys in the base plane of the 5° model traversed in a direction perpendicular to the upper surface of the base wedge. Details and dimensions of the rake are shown in Fig. 2. It should be noted that the Pitot tubes were parallel to the undisturbed base wedge flow but not parallel to the undisturbed side wedge flow. However, data[21] indicate only small errors due to pitot tube misalignment in hypersonic flow for angles up to about 8°. An electron beam flow visualization test showed no upstream distortion effects of the Pitot rake on the corner flowfield.

Test Conditions

Tunnel

The tests were conducted in the 22-in. helium tunnel of Langley Research Center.[22] Because of the possibility that

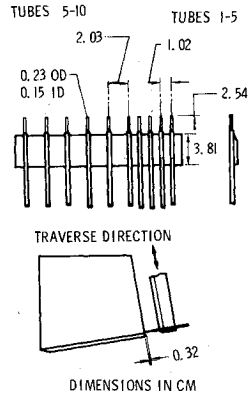

Fig. 2 Pitot rake arrangement.

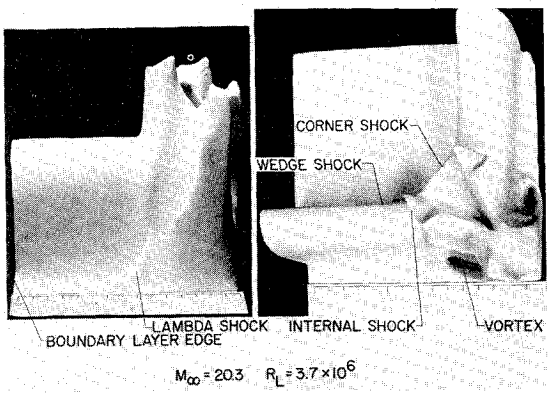

Fig. 3 Flowfield survey on 5° corner model.

the large size of the model might affect the freestream flow, Pitot and total temperature probes were mounted below the leading edge of the model, and checks on freestream flow conditions were made for runs in both heated and unheated flow. Freestream Mach numbers determined with the model in the tunnel were 19.0, 20.3, and 21.3 at stagnation pressures of 345, 690, and 1380 N/cm², respectively, independent of the stagnation temperature or wedge angle of the model.

Pressure distributions, oil-flow photographs, Pitot surveys, and electron beam photographs were made in unheated flow at a total temperature of 300°K. Heat-transfer studies were made at a nominal total temperature of 450°K. Reynolds numbers in heated flow were about 35% lower and $\bar{\chi}$ values about 26% higher than cold-flow values at the same stagnation pressure. The data of this investigation indicate that the resulting effects in the flowfields would be small.

Instrumentation

Pressures above 0.7 N/cm² were measured using unbonded strain-gage transducers; below 0.7 N/cm², variable capacitance transducers were used. Heat-transfer measurements were obtained using iron-constantan thermocouples spot-welded to a 0.025-cm-thick Inconel-X plate. A description of the electron beam apparatus used, as well as flow visualization photographs of several corner flow configurations, can be found in Refs. 20 and 23.

Tunnel Wall Boundary-Layer Interference

For all configurations, parts of the base and side wedges were immersed in the tunnel wall boundary layer. Estimates of the tunnel boundary-layer thickness at different stagnation pressures were made using the calibration Mach numbers determined with the models in the tunnel. The ideal gas area ratio for a given freestream Mach number gave a value of δ^*, which was multiplied by 2 to obtain δ. Reference 24 shows that δ is approximately twice δ^* for the wall boundary layer of this tunnel.

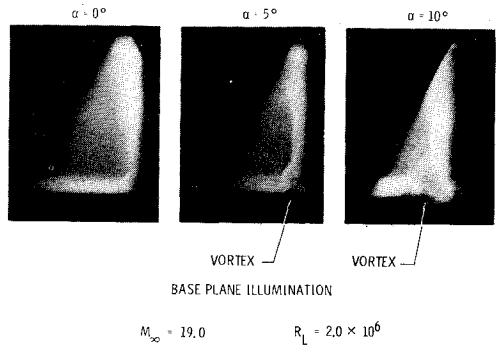

Fig. 4 Electron beam photographs.

Resulting values of δ were used to determine which instrumentation might lie within the tunnel wall boundary layer for a given model and run condition. Data points at these locations were omitted from the results of this investigation; the calculated boundary-layer edge is shown in oil-flow photographs and Pitot surveys presented herein.

Results and Discussion

A resumê of data obtained in the 22-in. helium tunnel follows, after which a discussion of the corner flowfield will be presented.

Mach 20 Data

Flowfield Pitot survey

Figure 3 shows a three-dimensional representation of the Pitot pressure in the base plane obtained by plotting Pitot pressure vertically on a base of the coordinates $\bar{z}/x$ and $\bar{x}/(x \cos 5°)$. (The base plane is not perpendicular to the upper surface of the side wedge.) The original pitot traces consist of slices parallel to the $\bar{y}/(x \cos 5°)$ coordinate; these were smoothed and a plaster cast made to produce the model shown in Fig. 3. Clearly visible are the wedge shock layers (regions of high constant Pitot pressure), a corner shock, the wedge boundary layers (regions of low Pitot pressure adjacent to the surfaces), and high pitot peaks in the region between the corner and the corner shock. Also visible are a weak disturbance extending through the boundary layer to the surface at $\bar{z}/x = 0.21$, and a low-pressure region surrounded by a thin layer of high Pitot pressure flow.

Electron beam photographs

An electron beam swept in a vertical plane at the base of the models illuminated a cross section of the flow in the sweep plane. The resulting visible cross sections, which appear similar to vapor screen condensation photographs, are shown in Fig. 4. In these photographs, bright regions correspond to regions of high density. Shock locations are clearly visible, including a central corner shock and internal shocks, especially for the 10° case. Also visible are what appear to be single vortices on the base plate for the 5° and 10° cases. Since the models are symmetrical, corresponding vortices should be seen on the vertical plates; however, because of the viewing angle, details of the vertical plate flow cannot be seen. No vortex is visible for the $\alpha = 0°$ case; however, a faint corner shock can be seen.

Surface pressure distributions

Measured surface pressure distributions at three Reynolds numbers are shown in Fig. 5. The data have been normalized by calculated laminar viscous-induced pressures for sharp plates and wedges, where values of P_W/P_∞ as a function

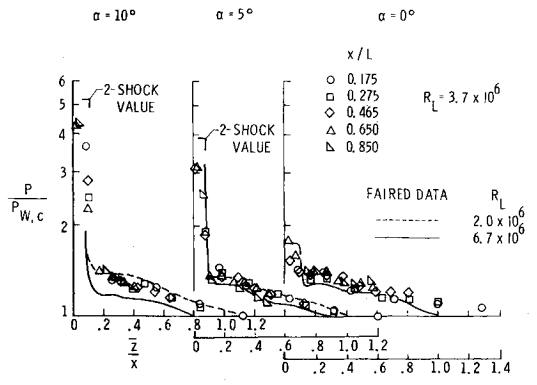

Fig. 5 Surface pressures at Mach 20.

of $G(\bar{\chi}/2)$ were taken from Ref. 25. Monaghan's equation[25] for G was used with $\gamma = \frac{5}{3}$ and $Pr = 0.688$:

$$G = 1.7208\left(\frac{\gamma-1}{2}\right)\left[\frac{T}{T_{aw}} + \frac{4.65\,Pr^{1/3} - 3.65Pr^{1/3}}{2.59}\right]Pr^{1/2} \quad (1)$$

where T_w is the surface temperature and T_{aw} the adiabatic wall temperature. The reference temperature values of density and viscosity were used in calculating C' using Monaghan's equation[26] for laminar T':

$$\frac{T'}{T_\infty} = A1\left[1 + \left(\frac{\gamma-1}{2}\right)M_\infty{}^2\right]\frac{T_w}{T_T} + \left[1 - A1 + A2\left(\frac{\gamma-1}{2}\right)M_\infty{}^2\right] \quad (2)$$

where

$$A1 = 1 - 0.468Pr^{1/3}$$

$$A2 = (1 - A1 - 0.273Pr^{1/2})Pr^{1/2}$$

The data are plotted in conical coordinates for all cases, even though such a coordinate system should not be applicable for the 0° case where viscous effects are large. Even so, this manner of presentation achieves a good degree of correlation in all cases.

Pressures about 4.2 times, 3.2 times, and 1.8 times local wedge pressure are measured for the 10°, 5°, and 0° cases, respectively, in the immediate corner region. A sharp pressure drop outside this region is followed by a compression, a local dip, and then a final approach to wedge pressure. Shown for the 5° and 10° cases are the pressure levels calculated using the simple two-shock method of Ref. 10. These values appear to be upper bounds on the inner pressure rise; interestingly, the calculated shock location is close to the experimentally determined edge of the high-pressure region.

Oil-flow photographs

Surface oil-flow patterns on $\alpha = 5°$ and 10° models are shown in Fig. 6. In both cases, a distinct pattern of s-shaped streak lines is thought to indicate the presence of vortices. Outside the s-shaped lines at $\alpha = 10°$, a featherlike pattern can be seen which is not visible at $\alpha = 5°$. Additional oil-flow studies have shown that the feather pattern appears at $\alpha = 5°$ with sufficient nose bluntness added.

Outside of the feather pattern at $\alpha = 10°$ and the s-shaped lines at $\alpha = 5°$, a strong crossflow region can be seen, terminating in an oil accumulation line. Beyond the oil accumulation line, the flow gradually approaches two-dimensional undisturbed wedge flow. No oil-flow photograph is available for the $\alpha = 0°$ case since the surface shear was too low to produce distinct oil-flow patterns within the Reynolds number range and run time of the tunnel.

Measurements made from the photographs of Fig. 6 indicate that the surface flow patterns are highly nonconical for

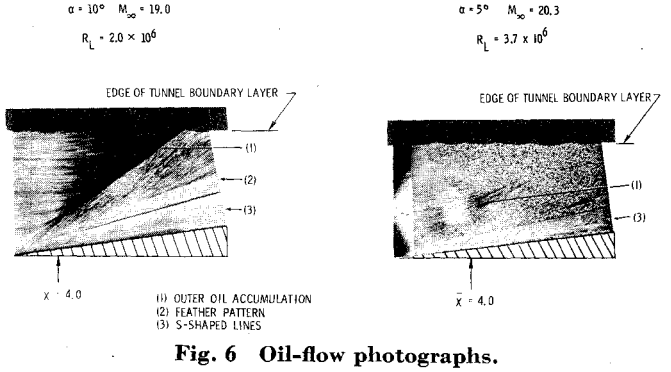

Fig. 6 Oil-flow photographs.

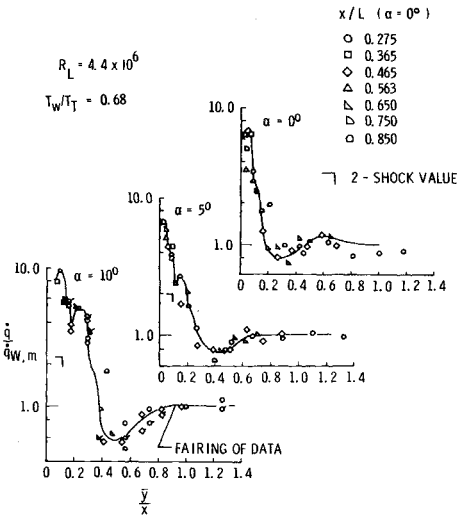

Fig. 7 Heat transfer at Mach 20.

values of $\bar{\chi}$ greater than about 4. For $\bar{\chi}$ less than 4, the patterns are nearly conical in nature, with the outer oil accumulation line and the beginning of the s-shaped curves showing somewhat faster growth than the outer edge of the s-shaped curves or the $\alpha = 10°$ feather pattern.

Heat-transfer distributions

Values of surface heat flux, normalized by the measured wedge heating value, are shown for the 0°, 5°, and 10°cases in Fig. 7. Calculated values of wedge heat flux were not used as normalizing parameters, since lateral conduction effects are present in the data. Starting transients in the 22-in. helium tunnel required that the data could not be reduced until 1 to 2 sec after the flow had started. The heat-transfer insert was heavily instrumented, and, because of the size of the disk calorimeter used, lateral conduction effects are significant after $\frac{1}{2}$ sec. An experimental investigation employing step heat inputs to the insert indicated that the conduction heating error was linear in time and nearly independent of the heating level for the rates encountered in the present tests. For this reason, the data are thought to represent correct trends.

The nearly conical nature of the flow is again evident by the correlation of the data at several x locations for a given angle of attack. A peak in heating occurs close to the corner in the region with the highest pressure. Estimates of the levels of peak heating which would occur due to a pressure rise alone were made for the 5° and 10° cases using the conservative two-shock pressure value and assuming $dp/dx = 0$. Measured peak heating is higher than these calculated values, actually about 10 times the local undisturbed wedge value at $\alpha = 10°$ and about 7 times wedge value at $\alpha = 5°$. Note that, as for the pressure distributions, the two-shock location predicts with fair accuracy the extent of the high heating region near the corner juncture. It has been shown in Ref. 12 that the ratio of peak heating to local laminar flat-plate heating is not constant at different x locations for symmetrically intersecting wedges at Mach 8. The present heat-transfer data are not detailed enough to determine whether or not this is the case at Mach 20.

Flowfield Analysis

In the following discussion, the symmetrical corner flow problem will be divided into two categories:

a) The first is the case of α greater than 0°, $\phi = 90°$, where strong wedge shocks interact and where, in the limiting case of inviscid flow, the flow is conical. Although viscous effects are significant at Mach 20, the observed conical nature

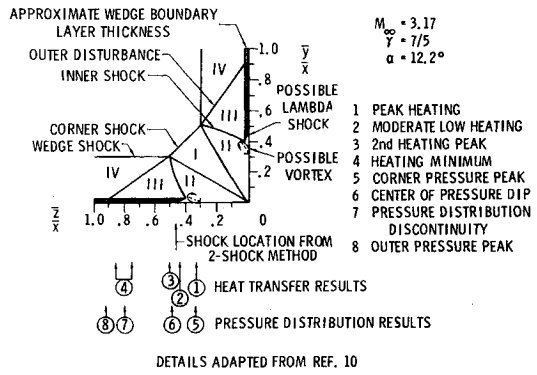

Fig. 8 Corner flow structure at Mach 3.17.

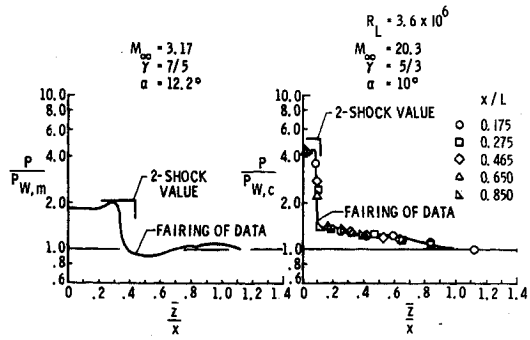

Fig. 10 Surface pressures at Mach 3.17 and Mach 20.

of the flow indicates that the inviscid interactions probably dominate the flow.

b) The second is the case of α equal to 0°, ϕ = 90°, where the flowfield is determined by viscous-inviscid interactions.

$\alpha > 0°$, $\phi = 90°$

Only two cases of published experimental data on symmetrically intersecting sharp leading-edge wedges are known to the authors: that of Charwat and Redekopp,[10] and that of Stainback and Weinstein.[12] Only Ref. 10 presents data in enough detail for an analysis of the flowfield to be made. Extensive results were obtained on a 12.2° corner model at Mach 3.17; however, limited results at other Mach numbers, wedge angles, and wedge intersection angles were presented.

Figure 8 shows a cross section of the flowfield on a 12.2° corner model at M = 3.17 in air determined from Pitot surveys, with results from the heat-transfer and surface pressure data shown. Noted in the figure are zones of flow described in Ref. 10 as follows:

Zone I: a region of conical flow bounded by slip lines and the corner shock.

Zone II: a region of complicated flow bounded by the slip lines and by a strong internal shock.

Zone III: an "outer interaction region" characterized by a compressive fan centered at the triple shock intersection point.

Zone IV: undisturbed wedge flow.

The Mach 20 flowfield on a 10° corner model is shown in Fig. 9, along with locations of features of the heat-transfer and pressure distribution data from the present study.

A flowfield feature common to both flows is the central region, Zone I. At Mach 3.17 this region is bounded by almost straight slip lines, whereas at Mach 20 the region is squeezed away from the corner by the presence of what appear to be large vortices. These vortices correspond to regions of high peak heating near the corner at Mach 20. The Pitot survey at Mach 3.17 contains a small region of low Pitot pressure near the location of peak heating. We conclude that this region of low Pitot pressure represents the core of a vortex which is the cause of high peak heating found in other corner flow data. Similar low Pitot pressure readings were found in the center of high-vorticity flow in the study of the flow behind delta wings at Mach 2.[27]

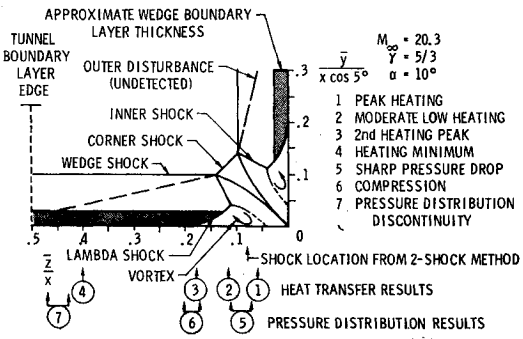

Fig. 9 Corner flow structure at Mach 20.

Away from the corner, a dip in heating corresponds closely to the outer edge of the vortex determined from the s-shaped lines of the oil-flow photographs and the extent of the low-pressure vortex core at Mach 20. Beyond the heat-transfer dip a second, lower peak in heating occurs, corresponding closely to the location where a disturbance extending through the wedge boundary layer strikes the surface. In this region, a featherlike pattern can be seen in the oil-flow photograph of the 10° corner model in Fig. 6. Such a pattern could be produced by counter-rotating vortices; however, the disturbance resembles one leg of a lambda shock in the Pitot survey on the 5° model. In the opinion of the authors of the present study, the disturbance is a lambda shock causing a local surface pressure compression at the point where it touches the surface, causing outflow in two directions. Whether or not this pattern appears in the oil-flow photographs would be a function of its strength and the thickness of the boundary layer through which it penetrates (a function of α for the test conditions of this study).

Beyond the boundary-layer disturbance, the heat transfer exhibits a gradual increase to wedge value. Near the region where wedge heating occurs, a discontinuity in the slope of the pressure distribution occurs, corresponding approximately to a line formed by the coalescence of the surface streaming oil. This oil accumulation line is the outer boundary of Zone III on the surface of the model. The boundary of Zone III in the flowfield was detected in the Pitot surveys of Ref. 10 but not in the present data.

From the preceding discussion, evidently the Mach 3.17 and Mach 20 flowfields exhibit gross similarities in internal and surface features. However, pressure distributions at Mach 20 do not exhibit the overexpansion found in Mach 3.17 data shown in Fig. 10. The data of Ref. 10 drop below wedge pressure, whereas those at Mach 20 are always higher, an effect probably attributable to thick boundary layers at Mach 20. Similarities are noted in the correspondence of three flow features common to both flows. Far from the corner, a dip in surface heat-transfer rate, the location of an oil accumulation line, and a slope change in the pressure distribution curve are closely related. This is the outer extent of the disturbance noted in Ref. 10 as bounding zone III. Outside this region, a gradual approach to wedge pressure and heating is found. Note that the two-shock value of pressure and shock location is a convenient outer bound in the high pressure near corner region at both Mach numbers.

$\alpha = 0°$, $\phi = 90°$

The greatest amount of data on any one corner flow configuration exists for sharp leading-edge flat plates intersecting at 90°. Stainback has published[2,6] pressure and

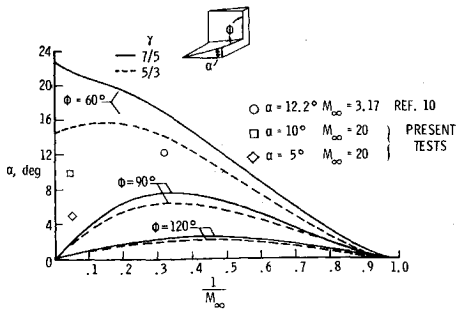

Fig. 11 Maximum wedge angles for possible shock intersections on symmetrical corners.

heat-transfer measurements at Mach 4.95 and heat-transfer measurements at Mach 8. Additional Mach 8 data in the form of peak heating rates and peak pressures have been published by Gulbran et al.[7] Cresci has measured surface pressures, heat-transfer rates, total temperature, and Pitot surveys in the flowfield at Mach 11.2 and Mach 11.8 in the strong interaction regime.[15,11] Bogdonoff and Vas[1] measured surface pressures at Mach 13.2, and Miller et al.[4] have measured surface pressures and heat-transfer rates at Mach 16.

At conditions where viscous effects are small, it is not clear whether a corner shock always occurs or whether, in some cases, the shocks cross. A simple analytic check of the occurrence of crossing shocks can be made for a conical symmetrical flow pattern, since crossing shocks can be treated as planar shocks reflecting in the plane of symmetry. This problem is equivalent to the shock reflection problem discussed in Ref. 28. The approach gives no consideration to the flow past the point of intersection, and so the method does not imply that the flow will accommodate to the surface boundary conditions with calculated possible shock intersection. Calculations for both air and helium are shown in Fig. 11 for intersection angles of 60°, 90°, and 120°.§ For wedge angles below the calculated curves, intersections can occur; above the curves intersections are not possible. For $\phi = 90°$ and above about Mach 3, as the Mach number increases, shock intersections are possible only at wedge angles below about 8°. Thus, thick boundary layers or large vortices at high Mach numbers which give rise to effective wedges could produce corner shocks. Conditions for the finite α cases of Ref. 10 and the present study, indicated on the figure, are outside the limit for shock intersection. It may be possible in some $\alpha = 0°$ cases for large viscous effects near the leading edge to induce a corner shock, after which, in the weak interaction region, a crossed shock structure could occur.

In an attempt to define surface features of the $\alpha = 0°$ corner flow in terms of heating rates, the Mach 8 heat-transfer results of Ref. 6 are plotted in conical coordinates and compared with Mach 20 results in Fig. 12. Reasonable correlation is obtained, indicating that the inviscid effects, although a direct result of viscous interference, are almost conical in nature. In both cases, the peak heating rates and heat-transfer minima lie close to the corner. No second peak in heating is found in either case indicating that lambda shocks, if present, are weak.

The theoretical analysis of the laminar corner boundary layer in Ref. 9 indicates that compressibility increases the extent of secondary flow within the boundary layer. This implies that vortex development, and thus peak heating rates, may be a function of the freestream Mach number. In order to determine what effect Mach number has on both peak heating rates and peak pressure for the 0° corner ($\phi = 90°$), available data from Mach 5 through the present results

§ Calculations supplied by Richard D. Wagner of Langley Research Center.

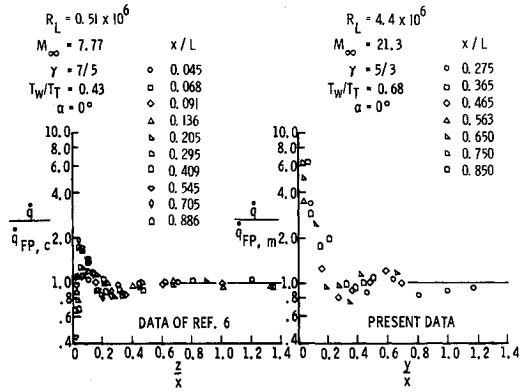

Fig. 12 Heat transfer at Mach 8 and Mach 20.

at Mach 20 are shown in Fig. 13. Peak heating rates shown in the figure are to be viewed as representative levels, since the magnitude of the peak heating would undoubtedly be a function of R and $\bar{\chi}$. Near the leading edge, at large $\bar{\chi}$ the shock-vortex system merges with the boundary layer, and peak heating rates would show x-wise variation. Away from the leading edge, Ref. 6 has shown that 0° corner peak heating at Mach 8 is a function of $(R_x)^{1/2}$, but invariant with x for finite α corners (within the range of the experiment). For some strong shock-vortex systems, it might be expected that 0° corner heating would exhibit the same trend as finite α corners.

Too little data exist for an attempt at correlation of all parameters; however, Fig. 13 shows the peak heating to be a strong function of Mach number, whereas peak pressures are influenced to a lesser extent. Evidently, simple boundary-layer pressure ratio analyses cannot predict peak corner heating rates.

Conclusions

From measurements of the flow characteristics over symmetrical sharp leading-edge corner flow models at Mach 20, the following conclusions are made:

1) The basic features of the flowfield previously observed at Mach 3 also occur at Mach 20, but are distorted by large vortices and thick boundary layers.

2) The flowfield on 5° and 10° corner models remains more or less conical in nature if the viscous interaction parameter $\bar{\chi}$ has values less than about 4. With $\bar{\chi}$ greater than 4, the flowfield is nonconical.

3) The presence of a vortex near the corner postulated by several authors has been found at Mach 20 in oil-flow and electron beam photographs and a flowfield survey. The vortex location coincides with the first peak in heating near the corner.

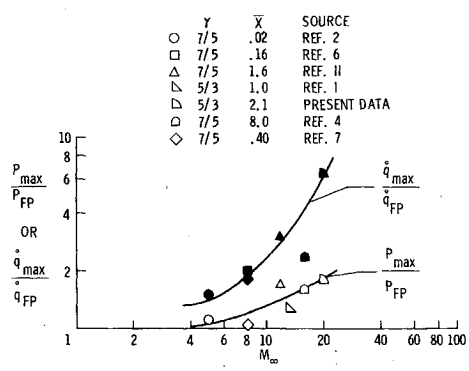

Fig. 13 Mach number effect on 0° corner maximum heating and pressure.

4) The second peak in heating coincides with a disturbance within the boundary layer originating from the internal shock and resembling one leg of a lambda shock.

5) Increasing Mach number increases the level of peak heating and corner pressure rise. At Mach 20, 10 times the undisturbed local wedge heating rates were observed in corners formed by 10° wedges. The peak heating level cannot be accounted for by the consideration of the peak pressure level only; i.e., a large portion of the increased heat transfer is evidently due to the influence of a localized vortical flow.

References

[1] Bogdonoff, S. M. and Vas, I. E., "A Preliminary Investigation of the Flow in a 90° Corner at Hypersonic Speeds, Part I—Flat Plates With Thin Leading Edges at Zero Angle of Attack," ARDC TR 57-202, AD 150-023, 1957, Bell Aircraft Corp., Buffalo, N. Y.

[2] Stainback, P. C., "An Experimental Investigation at a Mach Number of 4.95 of Flow in the Vicinity of a 90° Interior Corner Alined with the Free-Stream Velocity," TN D-184, 1960, NASA.

[3] Bloom, M. H. and Rubin, S., "High Speed Viscous Corner Flow," *Journal of the Aerospace Sciences*, Vol. 28, No. 2, Feb. 1961, pp. 145–157.

[4] Miller, D. S., Hijman, R., Redeker, E., Janssen, W. C., and Mullen, C. R., "A Study of Shock Impingements on Boundary Layers at Mach 16," *Proceedings of the 1962 Heat Transfer and Fluid Mechanics Institute*, edited by F. E. Ehlers, J. J. Kauzlaiich, C. A. Sleicher, Jr., and R. E. Street, Stanford University Press, Stanford, Calif., 1962.

[5] Wallace, J. and Clark, J. H., "Uniformly Valid Second-Order Solution for Supersonic Flow Over Cruciform Surfaces," *AIAA Journal*, Vol. 1, No. 1, Jan. 1963, pp. 179–185.

[6] Stainback, P. C., "Heat-Transfer Measurements at a Mach Number of 8 in the Vicinity of a 90° Interior Corner Alined with the Free-Stream Velocity," TN D-2417, 1964, NASA.

[7] Gulbran, C. E., Redeker, E., Miller, D. S., and Strack, S. L., "Heating in Regions of Interfering Flow Fields, Part I—Two- and Three-Dimensional Laminar Interactions at Mach 8," TR AFFDL-TR-65-49, Pt. I, 1965, The Boeing Co., Seattle, Wash.

[8] Rubin, S. G., "Incompressible Flow Along a Corner, Part I—Boundary Layer Solutions and Formulation of Corner Layer Problem," PIBAL Rept. 876, 1965, Polytechnic Institute of Brooklyn, N.Y.

[9] Libby, P. A., "Secondary Flows Associated With a Supersonic Corner Region," *AIAA Journal*, Vol. 4, No. 6, June 1966, pp. 1130–1132.

[10] Charwat, A. F. and Redekopp, L. G., "Supersonic Interference Flow Along the Corner of Intersecting Wedges," Memo. RM-4863-PR, 1966, The Rand Corp., Santa Monica, Calif.

[11] Cresci, R. J., "Hypersonic Flow Along Two Intersecting Planes," PIBAL Rept. 895 (AFOSR 66-0500), 1966, Polytechnic Institute of Brooklyn, N.Y.

[12] Stainback, P. C. and Weinstein, L. M., "Aerodynamic Heating in the Vicinity of Corners at Hypersonic Speeds," TN D-4130, 1967, NASA.

[13] Rudman, S. and Rubin, S. G., "Hypersonic Viscous Flow Over Slender Bodies Having Sharp Leading Edges," PIBAL Rept. 1018, AFOSR 67-1118, 1967, Polytechnic Institute of Brooklyn, N.Y.

[14] Korkegi, R. H., "A Limiting Condition for Supersonic Inviscid Interaction in the Corner of Intersecting Wedges," ARL-68-0099, 1968, Aerospace Research Labs., Tullahoma, Tenn.

[15] Cresci, R. J., Rubin, S. G., and Nardo, C. T., "Hypersonic Flow in Rectangular and Nonrectangular Corners," *AGARD Conference Proceedings No. 30*, 1968, Paper 18.

[16] Goebel, T. P., "A Theoretical Study of Inviscid, Supersonic Flow Along a Corner Formed by the Intersection of Two Wedges," Ph.D. thesis, 1969, Univ. of California, Los Angeles.

[17] Hains, F. D., "Supersonic Flow Near the Junction of Two Wedges," *Journal of the Aerospace Sciences*, Vol. 25, No. 8, Aug. 1958, pp. 530–531.

[18] Gessner, F. B. and Jones, J. B., "A Preliminary Study of Turbulence Characteristics of Flow Along a Corner," *Journal of Basic Engineering*, Vol. 83, No. 4, Series D, Dec. 1961, pp. 657–662.

[19] Bragg, G. M., "The Turbulent Boundary Layer in a Corner," *Journal of Fluid Mechanics*, Vol. 36, Pt. 3, May 1969, pp. 485–503.

[20] Bertram, M. H. and Henderson, A., Jr., "Some Recent Research With Viscous Interacting Flow in Hypersonic Streams," *Symposium on Viscous Interaction Phenomena in Supersonic and Hypersonic Flow*, May 7–8, 1969, Wright-Patterson Air Force Base, Ohio.

[21] Harvey, W. D., Bushnell, D. M., and Beckwith, I. E., "Fluctuating Properties of Turbulent Boundary Layers for Mach Numbers up to 9," TN D-5496, 1969, NASA.

[22] Arrington, J. P. and Joiner, R. C., Jr., "Longitudinal Characteristics of Several Configurations at Hypersonic Mach Numbers in Conical and Contoured Nozzles," TN D-2489, 1964, NASA.

[23] Weinstein, L. M., Wagner, R. D., Jr., Henderson, A., Jr., and Ocheltree, S. L., "Electron Beam Flow Visualization in Hypersonic Helium Flow," *1969 IEEE Third International Congress on Instrumentation in Aerospace Simulation Facilities*, 1969, Farmingdale, N.Y.

[24] Wagner, R. D., Jr., Maddalon, D. V., and Weinstein, L. M., and Henderson, A., Jr., "Influence of Measured Freestream Disturbances on Hypersonic Boundary-Layer Transition," *AIAA Journal*, Vol. 8, No. 9, Sept. 1970, pp. 1664–1670.

[25] Bertram, M. H., "Hypersonic Laminar Viscous Interaction Effects on the Aerodynamics of Two-Dimensional Wedge and Triangular Planform Wings," TN D-3523, 1966, NASA.

[26] Bertram, M. H., "Calculations of Compressible Average Turbulent Skin Friction," TR R-123, 1962, NASA.

[27] Boatright, W. B., "An Analysis of Pressure Studies and Experimental and Theoretical Downwash and Sidewash Behind Five Pointed-Tip Wings at Supersonic Speeds," Rept. 1380, 1958, NACA.

[28] Von Mises, R., *Mathematical Theory of Compressible Fluid Flow*, Academic Press, New York, 1958.